EurJIC
European Journal of Inorganic Chemistry

A Journal of
ChemPubSoc Europe

Accepted Article

Title: Flexible Ligand Based Lanthanide Three-Dimensional Metal-Organic Frameworks with Tunable Solid-State Photoluminescence and OH-Solvent-Sensing Properties

Authors: Germán Gomez, Elena Brusau, Anna Kaczmarek, Caroline Mellot-Draznieks, Joaquín Sacanell, Gwenaelle Rousse, Rik Van Deun, Clément Sanchez, Griselda Narda, and Galo Soler Illia

To be cited as: *Eur. J. Inorg. Chem.* 10.1002/ejic.201700099

Link to VoR: http://dx.doi.org/10.1002/ejic.201700099

WILEY-VCH

10.1002/ejic.201700099

WILEY-VCH

Flexible Ligand Based Lanthanide Three-Dimensional Metal-Organic Frameworks with Tunable Solid-State Photoluminescence and OH-Solvent-Sensing Properties

Germán E. Gomez*[a] [b], Elena V. Brusau[b], Anna M. Kaczmarek[c], Caroline Mellot-Draznieks[d], Joaquín Sacanell[e], Gwenaelle Rousse[f], Rik Van Deun[c], Clément Sanchez[g], Griselda E. Narda*[b], Galo J. A. A. Soler Illia*[h]

Abstract: Luminescent 3D metal-organic frameworks constructed by trivalent lanthanides (Nd^{3+}, Sm^{3+}, Eu^{3+}, Gd^{3+}, Tb^{3+}) and a flexible ligand (2-methylsuccinate) (**Ln-msucc**) have been hydrothermally obtained as polycrystalline solids. They were fully characterized by X-ray powder diffraction, thermal analysis, vibrational spectroscopy and scanning electron microscopy. The crystalline structure and topological features were elucidated and compared with those of related Ln-MOFs. The magnetic studies reveal that **Nd-msucc** and **Gd-msucc** present antiferromagnetic and ferromagnetic behavior respectively. Moreover, the solid state photoluminescence properties (SSPL) of all the compounds were fully explored. Depending on the lanthanide content, these materials exhibited luminescence performances in near infrared and visible regions. Particularly, the photophysical behavior of the Eu phase was exhaustively examined and the radiative and non-radiative constants and intrinsic quantum yields were calculated. The hypersensitive nature of Eu^{3+} $^5D_0 \rightarrow {}^7F_2$ transition allowed an in-depth study of the optical response in presence of various protic and aprotic solvents. As far as we know, the chemical-sensing studies employing **Eu-msucc** constitutes the first case reported for a lanthanide succinate-derived framework. The obtained results being promising for the elaboration of specific chemical sensors based on this material.

Introduction

Metal Organic Framework (MOF) materials have been the focus of a mature field with intense development due to their potential applications in catalysis [1], ion exchange and gas separation [2]. Moreover, the possibility of employing a diversity of building blocks, allows synthetic chemists to exploit specific an even tunable properties. In this context, lanthanide ions are of special interest in photonics and magnetism because of their unique properties which include characteristic narrow 4f-4f transitions (except La^{3+} and Lu^{3+}), a wide range of lifetime values and high quantum yields (QYs) [3]. These features are important qualities in the design of phosphors [4], the generation and amplification of light in lasers [5], optical amplifiers[3e, 6], solid-state lighting, full color displays and backlights [7]. Their *hypersensitive transitions* [8] enable Ln-MOFs to be suitable candidates for the construction of sensors for toxic substances [9] or physical variables such as temperature[10].

Flexible ligand based-MOFs (FL-MOFs) are characterized by possible rotational freedom within the linker giving rise to a variability in their conformations and consequently, opening the path towards different MOFs unique architectures. The flexibility of the linker is a key feature at the origin of fascinating properties such as "breathing" and "swelling" which are involved in selective sorption and controlled release of molecules from MOFs used in sensing and drug delivery, respectively [11]. Aliphatic linkers (succinate and adipate) have been used for the synthesis of lanthanide-based porous materials and further study of host-guest interactions[12,13]. In this sense, succinic acid has been presented as a model of flexible ligand for developing a variety of microporous Ln-MOF[14]. Particularly, succinate has been employed in combination with rigid

[a] Gerencia de Química, Centro Atómico Constituyentes, Comisión Nacional de Energía Atómica, Av. Gral. Paz 1499, 1650 San Martin, Buenos Aires, Argentina. *E-mail: gegomez@unsl.edu.ar
[b] INTEQUI – Instituto de Investigaciones en Tecnología Química, Facultad de Química, Bioquímica y Farmacia, Chacabuco y Pedernera, Universidad Nacional de San Luis, 5700 San Luis, Argentina. *E-mail: gnarda@unsl.edu.ar
[c] L3 – Luminescent Lanthanide Lab, f-element coordination chemistry, Ghent University, Department of Inorganic and Physical Chemistry, Krijgslaan 281, Building S3, 9000 Gent, Belgium.
[d] Laboratoire de Chimie des Processus Biologiques, UMR 8229 CNRS, UPMC Univ Paris 06, Collège de France, 11 Marcelin Berthelot, 75231 Paris Cedex 05, France.
[e] Depto. de Física de la Materia Condensada, Gerencia de Investigación y Aplicaciones, Centro Atómico Constituyentes, CNEA. Av. Gral. Paz 1499, San Martín, Buenos Aires, Argentina.
[f] Chimie du Solide et Energie, UMR 8260, Sorbonne Universités - UPMC Univ. Paris, Collège de France, 11 place Marcelin Berthelot, 75231, Paris Cedex 05, France.
[g] UMR 7574 Chimie de la Matière Condensée de Paris, UPMC Univ. Paris 06-CNRS, Collège de France, 11 place Marcelin Berthelot, 75231, Paris Cedex 05, France.
[h] Instituto de Nanosistemas. Universidad Nacional de San Martín. Av. 25 de Mayo 1021, San Martín, Buenos Aires, Argentina. *E-mail: gsoler-illia@unsam.edu.ar
Supporting Information (SI) available: [CIF file, powder XRD patterns, TG-DTA curves, FTIR spectra, and luminescence decay traces, spectra and transition Tables.]. See DOI: 10.1039/x0xx00000x

linkers to obtain mixed-ligand MOFs with interesting architectures and topological features[15]. In addition, it has been demonstrated in Ln-MOFs that the alkyl or aryl-substitution on the succinate backbone maintains the flexibility of the ligand. Depending on the synthetic conditions, phases with diverse dimensionalities were obtained using the asymmetric 2,2-dimethylsuccinic acid (H_2-2,2-dms) [16,17]. The choice of *meso* or a racemic mixture ± 2,3-dimethylsuccinate (H_2-2,3-dms) leads to the formation of two families of 3D MOFs along the lanthanide series with strong photoluminescence[17,18]. Recently, the exploration of 2-phenylsuccinic acid (H_2psa) as a flexible ligand, gave rise to only one series of 2D layered Ln-MOFs that behave as light emitters in the visible region [19] and efficient catalyts for cyanosilylation reactions[20].

With the aim to complete the studies on the influence of the alkyl-substitution on succinate-derived linkers and its impact on the resulting structures, we have carried out the synthesis of new phases obtained through the self-assembly of 2-methylsuccinic acid (H_2msucc) and lanthanides. Two examples of 2-methylsuccinate-based coordination polymers have been reported: a 3D [Mn(msucc)] MOF [21] and recently, 1D $[Ln(msucc)(NO_3)(H_2O)_2]\cdot H_2O$ and 2D $[Ln_2(msucc)_3(H_2O)_4]\cdot 3H_2O$ (Ln=Gd, Tb, Dy) coordination polymers[22].

In this work we present an isostructural family of photoluminescent 3D MOFs with formula $[Ln_2(C_5H_6O_4)_3(H_2O)_2]$ (Ln^{3+}=Nd, Sm, Eu, Gd, Tb) obtained by hydrothermal method. All compounds were fully characterized by X-ray powder diffraction (PXRD), vibrational spectroscopy (FTIR-Raman), thermal analysis (TGA-DTA-DSC) and scanning electron microscopy (SEM). Derived from the 4f transitions, magnetic susceptibility was explored in the 50-300 K range, and compared with analogous lanthanide frameworks. Additionally, the solid state photoluminescence (SSPL) properties were explored, including excitation-emission experiments, luminescence lifetimes measurements and europium intrinsic quantum yield (Q_{Eu}) calculations. Besides that, a quantification of the emitted light by CIE x,y (Commission Internationale de L'Éclairage) chromaticities was performed. Regarding the optical features of the Eu-phase, its chemical sensor activity was evaluated on the basis of the influence of diverse solvents on the hypersensitive $^5D_0 \rightarrow {}^7F_2$ signal as well as radiative and non-radiative constants (k_{rad} and k_{nrad}) and Q_{Eu}. All these studies set the basis for building of specific optical devises and could mark the route for the rational design of luminescent succinate-based Ln-MOFs.

Results and Discussion

Following the reaction shown in Scheme 1, polycrystalline samples were obtained as condensed "broccoli-like" bulk aggregates made of platy crystals of ~1x0.3x40 μm dimensions (yield=63-80% based on lanthanides), with high degree of twinning. This morphology, observed by SEM is shown in Figure 1.

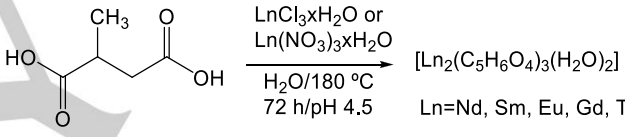

Scheme 1: Synthesis of **Ln-msucc** MOFs.

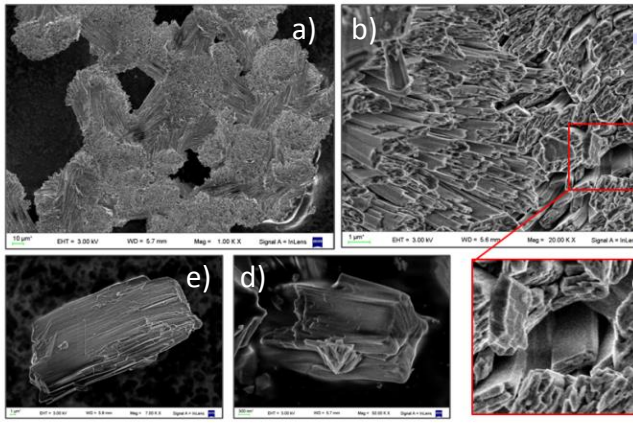

Figure 1: SEM micrographs of the "broccoli-like" bulk crystals (a) and a view of the platy habit (b and c) of **Tb-msucc**. The high degree of twinning is shown for **Tb-msucc** (d) and **Sm-msucc** (e) crystals.

Crystalline structural model for Nd-msucc

In the absence of single crystal data, the crystal structure of **Nd-msucc** was obtained with the assistance of computational methods as explained below. Relying on the similarity of its X-ray

powder diffraction pattern to those of the 2,3-dimethylsuccinate-based compounds such as **Sm-2,3-dms**[17](2,3-dimethylsuccinate), we anticipate that the newly synthesized frameworks should be very similar to those ones, particularly the nine-coordination number of the lanthanide. Along this line, the single crystal structure of **Sm-2,3-dms** (Pī space group, lattice parameters *a*=8.222(16) Å, *b*=12.342(3) Å, *c*=12.768(3) Å, α=117.50(3) °, β=93.64(3) °, γ=90.02(3)°, V=1146.29 Å^3) was used as the starting point to build an initial model of the **Nd-msucc** crystal structure. For the purpose of subsequent calculations, Sm atoms were replaced by Nd ones and one out of every two methyl groups of the linker was removed manually. Among the many possibilities, the methyl groups were removed to allow maintaining a maximum of stabilizing van der Waals contacts between the remaining methyl groups. The coordination sphere of each Nd atom was completed with one water molecule (4 H_2O molecules per unit cell in total).

This initial model was further geometrically optimized at the DFT level and confronted to the experimental X-ray diffraction pattern via an iterative process. The Rietveld method was first performed to refine the unit cell lattice parameters, which were then re-introduced into the DFT model for further structural optimization. This structure was then again implemented in the Rietveld refinement, and the result is shown in Figure 2. In this refinement, only peak shape parameters, coefficients of a 6-degree polynomia to describe background, preferred orientation parameters, a global angular shift and lattice parameters were allowed to vary. Indeed the complexity of the structural model (53 inequivalent atoms) and the broadening of the X-ray peaks prevent a complete refinement to be performed. Therefore, this model should be taken as likely but should be revised if single crystals become available in the future. The lattice obtained parameters were *a*= 8.487(3) Å, *b*=12.424(3) Å, *c*=13.030(2) Å, α=117.31(2)°, β=94.72(2)°, γ=94.82(3)°, and V=1205.11(6) Å^3. A preferred orientation along [001] was taken by using a modified March's function and indicates that crystallites adopt a platy habit perpendicular to [001].

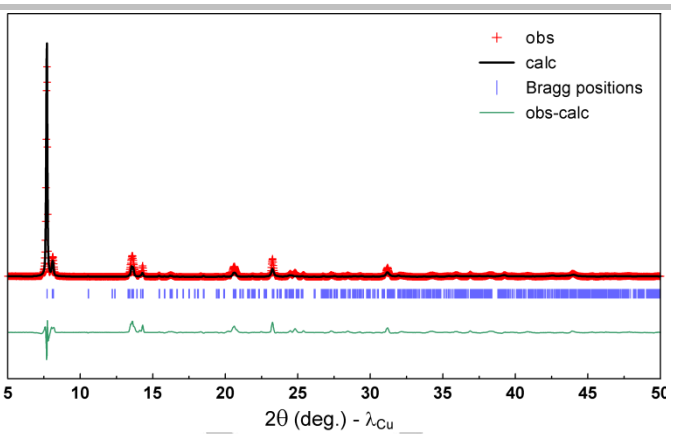

Figure 2: Rietveld refinement of laboratory X-ray diffraction pattern of **Nd-msucc**. The red crosses, black continuous line and bottom green line represent the observed, calculated, and difference patterns, respectively. Vertical blue tick bars are the Bragg positions.

Crystal Structures determination

The isostructural nature of all **Ln-msucc** was verified by comparison of the experimental PXRD patterns of the bulk materials with the simulated one from the **Nd-msucc** model (see Sup. Inf. S1).

The structural description is based on the crystal data of **Nd-msucc**. There are two crystallographically non-equivalent Nd^{3+} ions displaying nine coordination environment, and three independent **msucc** anions in the asymmetric unit (see Figure 3).

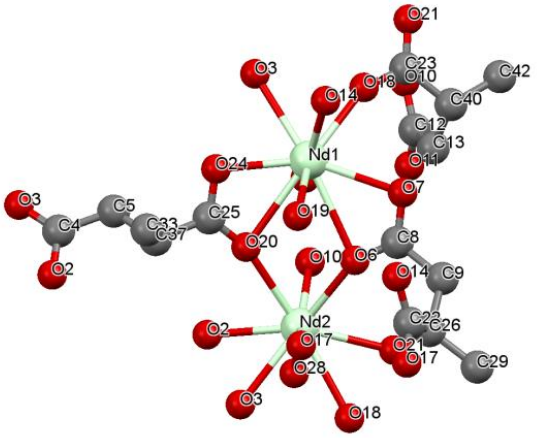

Figure 3: "Ball and stick" drawing of the asymmetric unit of **Nd-msucc** (green, red and gray balls represent neodymium, oxygen and carbon atoms, respectively. Hydrogen atoms were omitted for clarity).

Both Nd1 and Nd2 are surrounded by eight oxygen atoms belonging to carboxylate groups

and one oxygen atom of a coordinated water molecule. By analyzing the primary building units (PBUs) (Figure 4), the coordination geometry of both metal centers is consistent with a trigonal prism square-face tricapped [LnO_9] polyhedron (TPRS-9) [23]. The Nd1-O bond lengths fall in the 2.33- 2.82 Å range whereas the Nd2-O ones are in the 2.42 - 2.68 Å range which are consistent with those occurring in other lanthanide dicarboxylates[14,16-18].

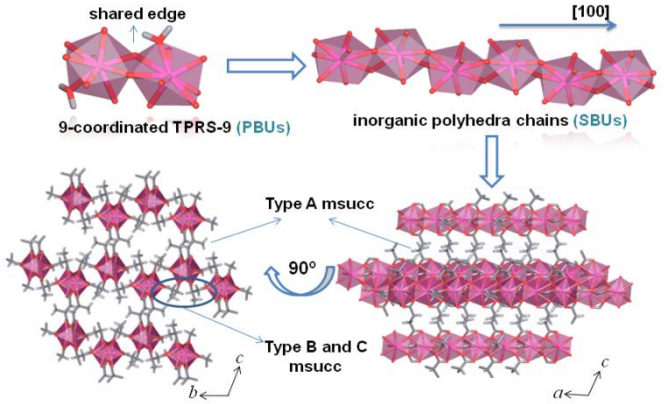

Figure 4: Representation of the PBUs and SBUs belonging to **Nd-msucc** (up). Views of the structure into the *ac* and *bc* crystallographic planes.

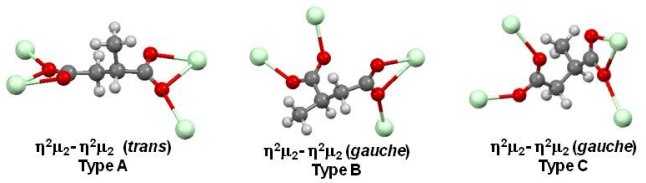

Figure 5: Representation of **msucc** coordination modes present in the **Ln-msucc** phases (green, red, gray and white balls represent neodymium, oxygen, carbon and hydrogen atoms, respectively).

Due the fact that methyl groups would not modify the flexibility of the linker, **Ln-msucc** structures are practically analogous to the previously reported **Ln-2,3-dms** phases.[18] The **msucc** ligand adopts the same conformation than that in **2,3-dms**: a *trans* conformation (Type A) [torsion angle (C25-C37-C5-C4), 176.95°], and two *gauche* conformations [torsion angles (C8-C9-C29-C22), -68.8° and (C23-C40-C13-C12), 63.4°] (Type B and C, respectively). Each ligand is connected to four metal ions; both carboxylate groups belonging to the *trans* conformer coordinate in the $\eta^2\mu_2$-$\eta^2\mu_2$ chelate-bridge mode whereas the *gauche* ones present the same coordination mode through one of the carboxylate groups and a bidentate-bridge mode through the other one (see Figure 5).

The Secondary Building Unit (SBU) consists of infinite chains of [NdO_9] edge-sharing TPRS-9 polyhedra (Figure 4) running along the *a* direction and connected by **msucc** Type B and C. The chains are linked along the *b* direction by the *gauche* ligands (Type B and C), while the *trans* ones (Type A) provide connection in the *c* direction. One weak H-bond interaction could be identified in the structure with a O···H distance of 2.7 Å, between one carboxylate group of a *gauche* **msucc** and the coordinated water molecule.

According to the connectivities displayed by the organic and inorganic sub-units in the structure, these MOFs may be classified as I^1O^2 nets where I^1 means that the inorganic connectivity is 1D and O^2 implies that the organic one is 2D since organic linkers connect the SBUs in two directions. The overall dimensionality of the structure is 3D as the sum of the exponents. [24]

The TOPOS[25] software was employed to obtain the topological simplified representation of the **Ln-msucc** compounds (Figure 6). The frameworks can be described in terms of the rod-shaped SBU packing. [26] Thus, an intermetallic centroid may act as 5-connected node, acquiring three connections to carboxylate groups and two bonds to adjacent Ln^{3+} ions, resulting in a hexagonal **bnn** type net with point symbol ($4^6.6^4$). [27] The same topology was obtained for isomorphic phases **Ln-succ** (Ln=La-Gd)[14j], **Ho-succ**[16] and **Ln-2,3-dms** (La[17], Pr-Eu[18]) (see Sup. Inf. S2).

The influence of the methyl substituents in the succinate backbone does not seem to affect the resulting Ln-MOFs frameworks when selecting **msucc** or **2,3-dms** as organic linkers under similar synthetic conditions. It is highlighted that **Ln-succ** (La-Gd and Ho) (References 14j and 16), **Ln-msucc** and **Ln-2,3-dms** (Ln=Nd-Eu)[18] crystallize in the same S.G. (Pī), with structural similarities such as the linkers' coordination modes and the net topology. Besides that, the methyl substituents on succinate do not alter substantially the ligand

flexibility, since the *gauche* and *trans* conformers are presented in a 2:1 ratio respectively, evidencing a predominant *gauche effect*[14e].

An analysis of the microporous nature of **Ln-msucc** compounds was carried out using PLATON [28] and CrystalExplorer [29] packages. According to this study, the 3D compounds exhibit large 1D channels along the *a* direction with a calculated void volume of 132 Å^3 per unit cell (equivalent to 17.7% of the unit cell) (see Figure 6). This value matches well with the decreasing trend of the micropores volume as the linker's size increases from **Ln-succ** to **Ln-2,3-dms** 3D frameworks (Figure 7). In this sense, the presence of one or two methyl groups oriented toward the unidimensional channels results in a decrease of a ~48% or 80%, respectively, of the accessible volume with respect to the maximum void space reported for **Ln-succ** (P$\bar{1}$)[14j].

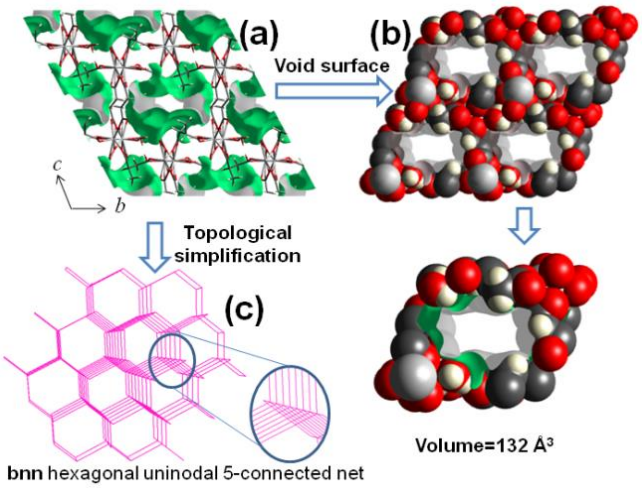

Figure 6: Crystal void (a) and void surface representation (b) for **Nd-msucc** using CrystalExplorer.[41] Topological simplification of the **bnn** network of **Nd-msucc** (c).

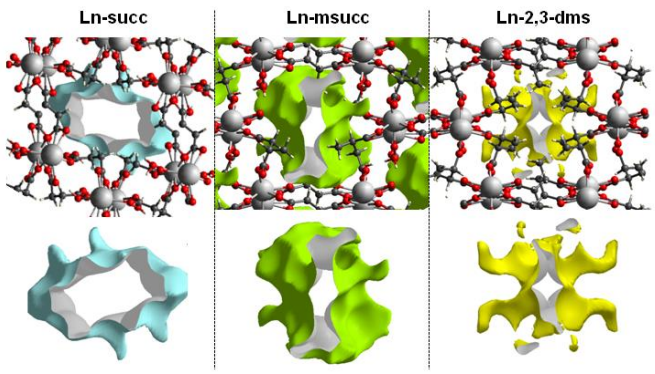

Figure 7: Crystal voids representation for **Ln-succ**[14j], **Ln-msucc** and **Ln-2,3-dms**[18] along *a* direction using CrystalExplorer program.[41]

Vibrational behavior and thermal properties

Regarding the isostructural nature of all compounds, **Sm-msucc** was selected as model to describe their vibrational and thermal properties (Sup. Inf. S3). The interpretation of the FTIR spectra was performed by considering the most important internal vibrations of water molecules, carboxylate and methyl groups and their comparison with those observed in **Ln-2,2-dms**[16,17] and **Ln-2,3-dms** series[17,18, 30]. The corresponding assignment of bands is shown in Sup. Inf. S4.

Ln-msucc show similar profiles and a slightly higher thermal stability respect to **Ln-2,3-dms** (P$\bar{1}$) phases (decomposition temperature range 361.6-463.3 °C and 320-415 °C, respectively). The thermal data for all the compounds are summarized in Sup. Inf. S5; Δm % values calculated on the basis of the determined stoichiometries show a good agreement with the experimental ones. The dehydration process is associated with an endothermic signal in the DTA or DSC curves. Thermal evolution proceeds with the decomposition of the **msucc** linkers through several steps leading to the formation of the corresponding oxides. The corresponding mass decays are accompanied by strong exothermic DTA or DSC peaks.

Magnetic Properties

The study of the magnetic field effect on the materials properties, particularly in magnetic phase transitions can help to support their behavior by varying the temperature. The temperature dependence of the magnetic susceptibility for **Nd-msucc** and **Gd-msucc** is shown in Figure 8, as χ_M.T (black traces) and χ_M^{-1} (red traces). The values are calculated per mol of Nd and Gd atom, respectively. The χ_M.T value for **Nd-msucc** at 300 K is 1.76 emu.K/mol, it is very close to the expected value for the isolated Nd^{3+} ions with a $^4I_{9/2}$ ground state[31]. We observe that χ_M·T decreases on reducing temperature, a fact that can be related with the antiferromagnetic ordering of Nd^{3+} ions. The linearity of χ_M^{-1} indicates that the susceptibility follows the Curie-

Weiss law, C/(T-θ), with C = 2.02 emu.K/mol and θ = -57(1) K. Similar temperature dependence was observed for flexible 3D Nd-adipates, previously synthesized by us[32,33]. The negative value of θ also indicates an antiferromagnetic interaction. For **Gd-msucc** (Figure 8 down), the χ_M also follows the Curie-Weiss law with C = 6.43 emu.K/mol and θ = -2 K. χ_M·T departs from a value of 6.5 emu.K/mol at 300 K, which is slightly smaller than that corresponding to isolated Gd^{3+} ions with a $^8S_{7/2}$ ground state[31], and remains almost constant on lowering temperature. The small upturn of χ_M·T at low temperatures can be ascribed to a weak ferromagnetic interaction between Gd^{3+} ions, as stated by other authors for mixed-ligand based MOFs[34,22].

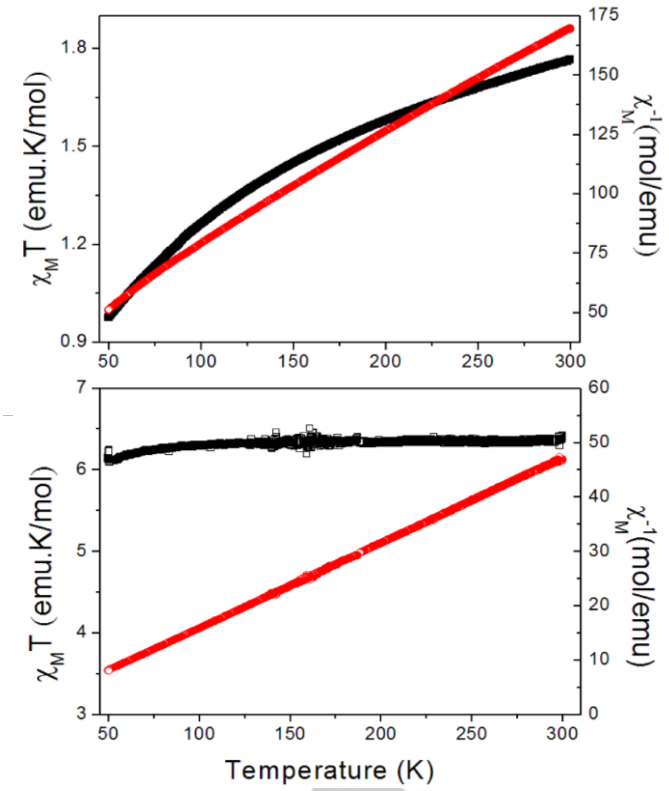

Figure 8: Temperature dependence of χ_M·T (black) and χ_M^{-1} (red) for **Nd-msucc** (up) and **Gd-msucc** (down) measured between 50 and 300 K under the application of a magnetic field of 1 Tesla.

SSPL (Solid State Photoluminescence Properties)

Specific reports[35] tend to define basic procedures that should be followed by researchers with the purpose of exploring the PL properties of optically active MOF materials. These studies include parameters such as a) PL spectra, b) QYs and, c) observed lifetimes (τ_{obs}) values. Besides, the quantification of the emitting light is relevant to elaborate optical devices as chemical[9] and physical sensors [36]. In this context, room temperature SSPL properties of **Ln-msucc** were explored here and compared with those of analogous Ln-MOFs. Moreover, a thorough study concerning the photophysical features of the Eu-phase was performed.

By monitoring the emission at 1061.0 nm (9425 cm^{-1}) and varying the excitation wavelength between 250 and 850 nm, a multi-peak excitation spectrum was recorded for **Nd-msucc**, as can be seen in Figure 9. Peaks labeled a-k are assigned to the corresponding transitions within the Nd^{3+} ion's 4f shell. Upon excitation at 578 nm (17301 cm^{-1}) in the $^2G_{7/2}$, $^4G_{5/2}\leftarrow{}^4I_{9/2}$ levels, the typical narrow Nd^{3+} emission peaks in the near infrared (NIR) region are observable. The peaks labeled l-n are assigned to the electronic transitions $^4F_{3/2}\rightarrow{}^4I_J$ (J=9/2, 11/2 and 13/2) (Sup. Inf. S6). Upon excitation at 355 nm, the emission at 1061.0 nm shows a mono-exponential decay profile, with a τ_{obs} of 0.83 μs (see Sup. Inf. S7).

At λ_{exc}= 402 nm ($^6P_{3/2}\leftarrow{}^6H_{15/2}$), **Sm-msucc** shows the characteristic Sm^{3+} orange emission with peaks centered at 561, 594, 641 and 704 nm (Figure 9), assignable to the $^4G_{5/2}\rightarrow{}^6H_J$ (J=5/2, 7/2 9/2 and 11/2) electronic transitions (see Sup. Inf. S6), similarly to **Sm-succ**, **Sm-2,3-dms** and **Sm-psa** (2-phenylsuccinate) compounds. The corresponding luminescence decay profile is given in Sup. Inf. S8; the experimental curve could be fitted with a mono-exponential decay equation and the calculated τ_{obs} value is 5.57 μs. The intensity of the emission and the τ_{obs} of **Sm-msucc** are the highest ones in comparison with analogous succinate phases[14j,18,19].

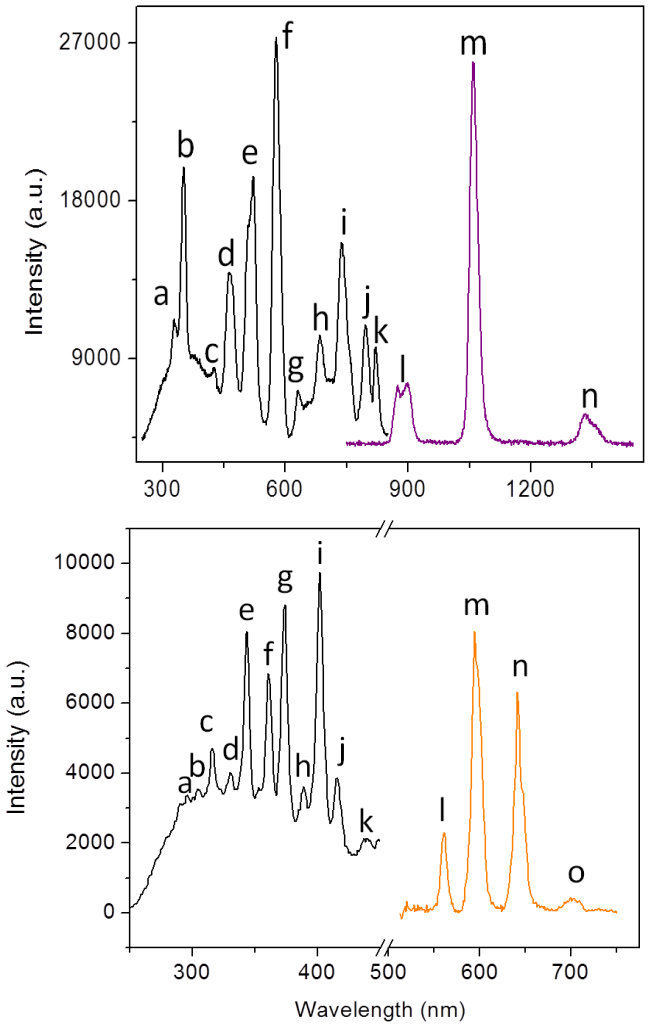

Figure 9: Excitation (black traces) and emission spectra of **Nd-msucc** (up) and **Sm-msucc** (bottom).

The excitation spectrum of **Gd-msucc** exhibits two broad bands ascribed to n→n* transitions from the carboxylate moieties of the **msucc** linkers. Upon UV excitation (λ_{exc}=356 nm, 28090cm^{-1}), a blue emission with a maximum centered at 439 nm (22779 cm^{-1}) is observed (label c, in Figure 10). Due the fact that the $^6P_{7/2}$ state of Gd^{3+} lies at too high energy to be populated by most organic linkers, the emission can be related to n*→n transitions from the **msucc** linkers (*ligand-centered emission*). Similarities in the optical behavior of **Gd-msucc** were found when it is compared with other succinate frameworks. For example, Zhou and col[14e]. reported two dense Gd^{3+} 3D MOFs based on succinic acid, **Gd-succ1** (Pī) and **Gd-succ2** (C2/*c*) with ligand blue-greenish emissions. Recently, we reported a 2D MOF based on the **psa** aromatic linker[20] (**Gd-psa**) exhibiting a strong blue-green luminescence centered at 441 nm. The spectrum of **Gd-msucc**, in comparison with that of **Gd-psa** is 2.5 times lower in intensity (Sup. Inf. S8). This fact can be explained by two reasons: i) the absence of the π electronic density in the linker (the most likely fact), and ii) the presence of two water molecules per asymmetric unit in **Gd-msucc**, which could quench the luminescence by *multiphonon relaxation* mechanism of OH groups[37].

The excitation spectrum of **Tb-msucc** was recorded in the 250 – 525 nm range, monitoring the $^5D_4 \rightarrow {}^7F_5$ emission at 543 nm (Figure 10). The narrow peaks labeled a-k in the excitation spectrum correspond to transitions within the Tb^{3+} ion's 4f shell. Under direct excitation into the 4f levels ($^5L_{10} \leftarrow {}^7F_6$, 368 nm), the typical narrow Tb^{3+} peaks, yielding a yellowish green emission, are observed. The corresponding assignment of the excitation $^{2S+1}L_J \leftarrow {}^7F_6$ and the emission $^5D_4 \rightarrow {}^7F_J$ (J = 6-0) electronic transitions is shown in Sup. Inf. S6. The most intense emission peak located at 543 nm shows a monoexponential decay profile (Sup. Inf. S7) with a τ_{obs} of 1.46 ms. When SSPL performances of other related Tb-MOFs are compared with those of the **Tb-msucc**, some trends could be find, such as the τ_{obs} that decreases according to τ_{obs}**Tb-2,3-dms**>τ_{obs}**Tb-psa**>τ_{obs}**Tb-msucc**, being a clear correlation between water content into the structures and *multi-phonon relaxation*[49] (Sup. Inf. S8).

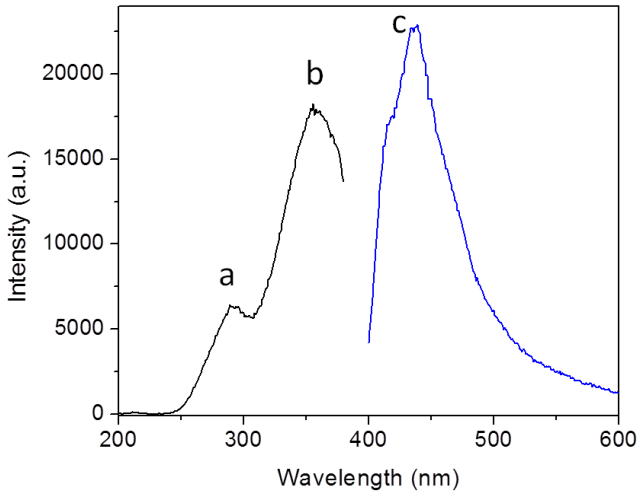

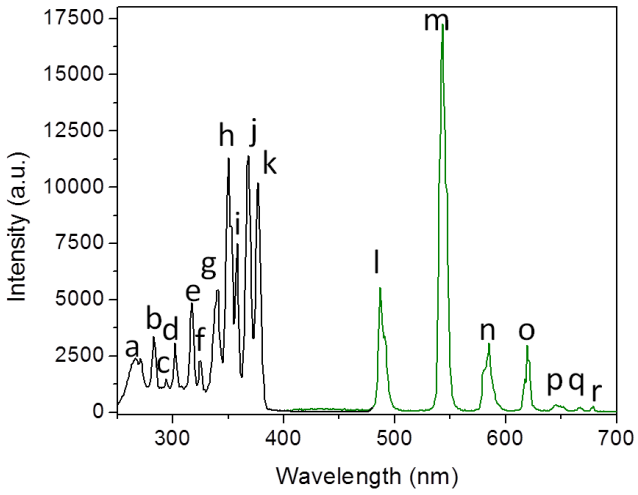

Figure 10: Excitation (black traces) and emission spectra of **Gd-msucc** (up) and **Tb-msucc** (bottom).

Eu-msucc shows the well-known red europium luminescence. The excitation and emission spectra are given in Figure 11 and the assignment of the observed electronic transitions can be found in Sup. Inf. S6. As it was determined for Nd, Sm and Tb-phases, the luminescence of **Eu-msucc** can be obtained by direct excitation into the $^{2S+1}L_J$ electronic energy levels, yielding *lanthanide-centered luminescence*. Upon excitation at 392 nm (25510 cm^{-1}), $^5D_0 \rightarrow {}^7F_J$ (J =0–4) transitions in the 500 - 750 nm range were identified. The luminescence decay time was calculated from the decay trace monitoring the $^5D_0 \rightarrow {}^7F_2$ emission (see Sup. Inf. S7). The corresponding decay curve was fitted with a single exponential function, this parameter being unable to distinguish in this case between two lanthanide centers in a very similar chemical environment. However, the splitting in the hypersensitive $^5D_0 \rightarrow {}^7F_2$ transition (inset Figure 11) supports the crystallographic data. The resulting τ_{obs} of 0.653 ms is almost five times higher compared with the starting material $Eu(NO_3)_3$[38].

The hydration number (n_w) in crystalline Eu^{3+} compounds can be estimated from the observed lifetime in ms (τ_{obs})[39], (see equation 1 in Sup. Inf. S9). The n_w value for **Eu-msucc** is 0.908, which is in agreement with the structural data where one water molecule is coordinated to each metallic center.

In order to evaluate the PL efficiency, the europium intrinsic quantum yield (Q_{Eu}) was calculated. This parameter expresses how well the radiative processes (k_{rad}) compete with the non-radiative (k_{nrad}) ones, particularly in lanthanide systems[40]. These two pathways are essentially involved in the depopulation of $^5D_0$ state, as it is expressed in Sup. Inf. S9 (Equations 2-6). The complete SSPL parameters for **Eu-msucc** are summarized in Sup. Inf. S10.

When the optical behaviors of **Eu-msucc** and **Eu-2,3-dms** are compared, τ_{obs} and Q_{Eu}% of the former MOF are higher than those of the **Eu-2,3-dms**. Taking into account that both Eu-MOFs have the same water content and similar structural features, the results suggest that an additional –CH_3 group affects the SSPL properties, due to C-H oscillators quenching. The higher k_{nrad} in **Eu-2,3-dms** respect to **Eu-msucc** (1562 s^{-1} *vs* 1193.6 s^{-1}) supports this trend. This fact also explains the higher intensity reported for **Eu-succ**[14j] which does not present methyl quenching contribution[41].

The quantification of color emission (QC) of different luminescent materials allows their comparison by studying the corresponding light-emitting performance. In this sense, the color coordinates are usually calculated using the CIE x,y chromaticities[42] system and plotted in a two dimensional diagram (Sup. Inf. S11). The color emission of **Sm-msucc**, **Eu-msucc**, **Gd-msucc** and **Tb-msucc** were quantified in terms of x,y color coordinates as displayed in Figure 11. Except for **Gd-msucc**, the remaining MOFs present *lanthanide- centered luminescence* without ligand sensitization; for this reason the x,y coordinates are close to those of MOFs such as **Ln-2,3-dms**[18] and **Ln-psa**[20] (see Sup. Inf. S12). S13 in Sup. Inf. summarizes the SSPL in the visible range of various succinate-type frameworks.

The photophysical characterization data of all of the **Ln-msucc** compounds are shown in Table 1. According to this information, it is possible to establish criteria for the design of multifunctional luminescent materials. In this sense, technological applications that require fast optical response such as scintillation [43] and displays involve small lifetime values. For this reason **Nd-msucc** or **Sm-msucc** could be employed to elaborate devices working in the NIR and visible region,

respectively. Besides, owing to their strong luminescence, pure red or green colors, and long lifetimes, **Eu-msucc** and **Tb-msucc** are promising candidates for photoluminescent sensors.

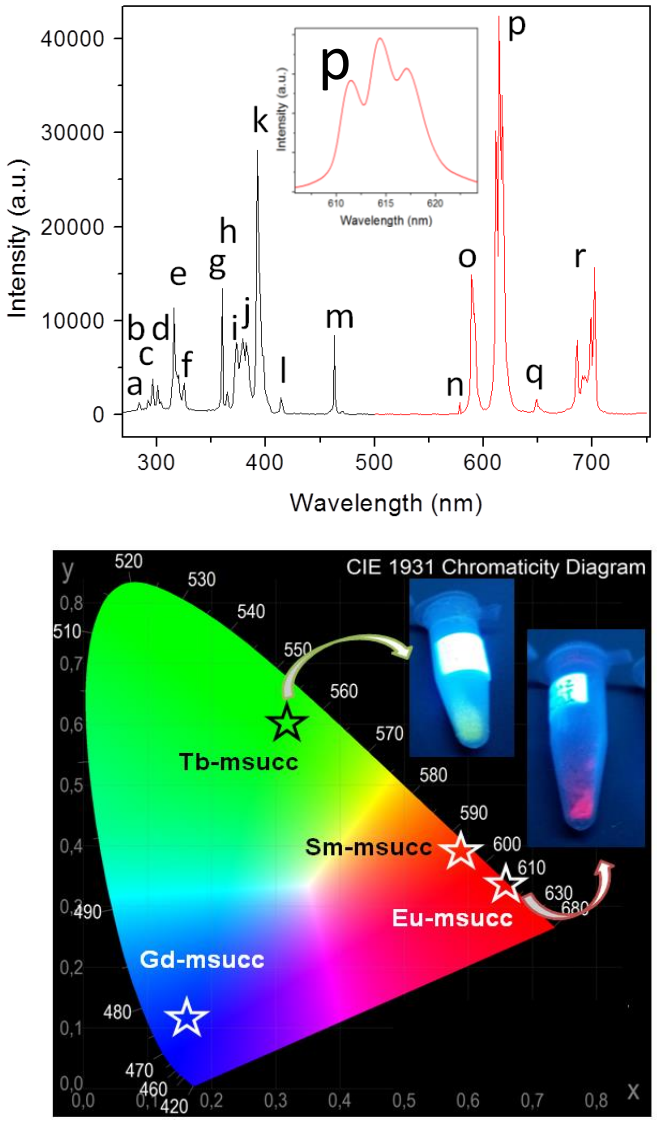

Figure 11: Excitation (black trace) and emission spectra of **Eu-msucc** (up). CIE 1931 chromaticity diagram showing the (x,y) color coordinates for **Sm-msucc**, **Eu-msucc**, **Gd-msucc** and **Tb-msucc** after being excited with the corresponding wavelength. The picture shows **Eu-msucc** and **Tb-msucc** samples after irradiation with a portable UV lamp (bottom).

Table 1. Summary of the photophysical features of **Ln-msucc** compounds at room temperature.

Ln-msucc	τ_{obs}	Q_{Ln}%	Color emission
Nd-msucc	0.83 μs	-	Red (NIR)
Sm-msucc	5.57 μs	-	Orange
Gd-msucc	-	-	Yellowish green
Tb-msucc	1.46 ms	-	Green
Eu-msucc	0.653 ms	22.06	Red

In the context of chemical sensor design, Tb^{3+} and Eu^{3+} inorganic compounds have been the focus of interest due to their *hypersensitive transitions* that provide PL properties which are extremely affected by the chemical [44] and physical environment.[8b] During the last fifteen years, Eu and Tb-MOFs have been extensively used as unique platform for sensing water [45], ions [46], VOCs [47] (volatile organic compounds) and hazardous molecules such us explosives[48].

With the purpose of investigating potential applications in chemosensing, five protic (water, methanol, ethanol, n-butanol and isopropanol) and three aprotic solvents (DMF, chloroform, acetone) were chosen to study the sensor performance of **Eu-msucc** through PL measurements, in comparison to its corresponding SSPL. **Eu-mscucc** was selected because of its strong 4f luminescence even without the presence of aromatic moieties in the linker. For a quantitative study of the possible energy transfers, fluorescence measurements were carried out as it is detailed in the Experimental Section. Exciting the suspension samples at 392 nm, the typical Eu^{3+} transitions are observed, the $^5D_0 \rightarrow {}^7F_2$ transition being the most intense one. Differences in intensity values have been seen in both sets of excitation and emission spectra (see Figure 12). Indeed, the $^5D_0 \rightarrow {}^7F_2$ transition intensity strongly depends on the solvent and particularly water, produces a significant quenching effect.

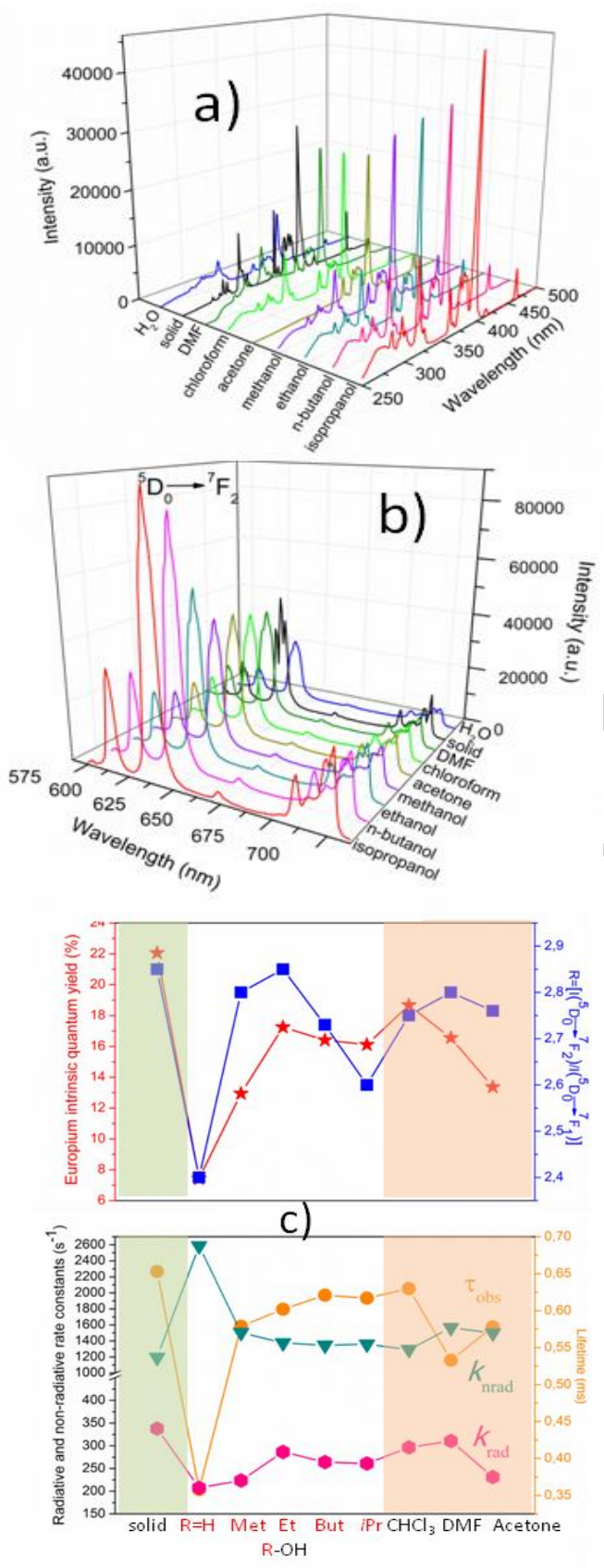

Figure 12: Excitation (a) and emission spectra (b) of the **Eu-msucc**-solv systems (λ_{exc}=392 nm). Comparison of PL parameters of **Eu-msucc** in different solvents (c).

The R value, defined as $I(^5D_0\rightarrow{}^7F_2)/I(^5D_0\rightarrow{}^7F_1)$, is an approximation that provides information about the electronic environment of Eu^{3+} ion in diverse inorganic compounds. As it can be seen in Figure 12a, the signals dramatically change in water and isopropanol (*i*Pr-OH), with strong intensity decrease or enhancement respectively, and with the observable modifications in the R values. With other solvents, the R values are close to that obtained in the solid state, indicating that the coordination environment of **Eu-msucc** is maintained.

Nevertheless, for a physico-chemical analysis it is necessary to study other PL parameters such as k_{rad} and k_{nrad} constants, QYs and τ_{obs}. Figure 12c (and Sup. Inf. S10 and S14) shows the PL parameters of **Eu-msucc** in various solvents.

Analyte-lanthanide ion interactions may be inferred from the determination of energy transfer efficiency (η_{ET}) within the frame of Förster's dipole-dipole mechanism. In this case, the following equation is useful to estimate the efficiency of transfer between the donor and the acceptor.[49]

$$\eta_{ET}=1-(\tau_{obs}/\tau_0)$$

where τ_{obs} and τ_0 are the lifetimes of the donor (**Eu-msucc**) in presence and in absence of the acceptor agents (solvents), respectively. The mechanism of PL quenching by coupling vibrations is based on the ability of certain atomic groups to consume part of the energy during the energy transfer (ET) process.

Such quenching effect can be assessed by the so called "quantum numbers"[50] (number of times for such vibrational stretching to match up the 4f-electronic transition). In this case, the $^5D_0\rightarrow{}^7F_2$ transition energy (16287 cm^{-1}) is about 4.5 times that of O-H (3650 cm^{-1}), 6 times that of C-H (2960 cm^{-1}) and 10 times that of C=O (1680 cm^{-1})[42] (see Jablonski diagram in Figure 13). The lower the quantum number is, the higher the efficiency of the quenching effect, so O-H groups are more efficient than other organic groups to produce quenching. This observation matches well with the η_{ET}% values (inset Figure 13),

where **Eu-msucc** exhibits the highest values in aqueous media, methanol (O-H), DMF and acetone (C=O and C-H groups).

Moreover, the decrease in k_{rad} indicates a quenching of Eu^{3+} signals due to O-H groups from water molecules of the environment, taking place through non-radiative pathways. When PL properties of **Eu-msucc** in alcohol media are compared with those in water, certain tendencies could be identified: the shorter the aliphatic chain of linear alcohols is, the higher the quenching effect is. These results indicate a size-solvent dependence quenching process due to interactions with lanthanide centers through 1D-channels, as it was seen in previous porous Eu-MOFs[51] probed for small molecules. The quenching effect of acetone seems to follow the same dependence. Despite its size, the absence of suitable oscillators in $CHCl_3$ prevents significant emission deactivation by this solvent. In comparison with the PL performance in the solid state, a remarkable decrease of radiative processes (and an increase in non-radiative constants) is observed in acetone (see Figure 12c). Some authors have justified this kind of quenching of 4f-signals in Ln-MOFs by diffusion-controlled mechanism.[52]

These preliminary results set the basis for the elaboration of solvato-sensors based on lanthanide compounds, specifically for vapour pressure detection devises (i.e., humidity).

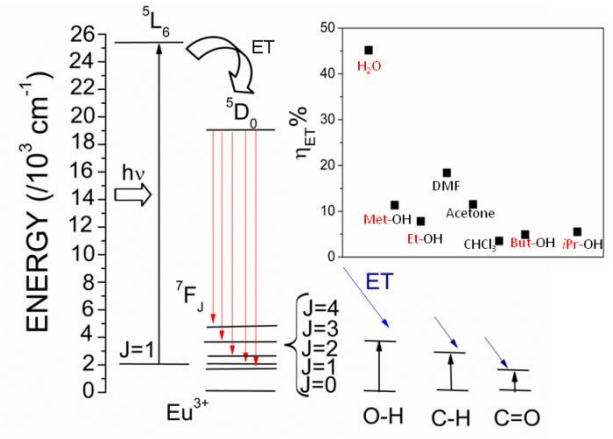

Figure 13: Modified Jablonski diagram showing the energy levels of Eu^{3+} ions (ET = energy transfer; black arrow=excitation process; red arrows= 4f emissions; blue arrows= energy transfers from 4f levels to organic groups) and the vibrational quenching effects of organic groups. Inset: Calculated energy transfer efficiencies of **Eu-msucc** in different solvent media.

Conclusions

New FL-Ln-MOFs (Ln^{3+}= Nd, Sm, Eu, Gd and Tb) based on the flexible 2-methylsuccinate ligand have been hydrothermally obtained and fully characterized. The 3D MOFs are isostructural and belong to a triclinic structure (Pī space group) where each metal center is nona-coordinated. The presence of *gauche* and *trans* conformations of **msucc** in the frameworks accounts for the flexibility encountered in succinate-based MOFs. The structures were topologically simplified as hexagonal **bnn** type nets. The magnetic properties **Nd-msucc** and **Gd-msucc** were explored and compared with analogous FL-MOFs, revealing an antiferromagnetic and ferromagnetic behavior, respectively. Also, an exhaustive photophysical characterization which involved excitation-emission experiments, calculation of lifetime values, Eu^{3+} intrinsic quantum yields and quantification of emission light color was carried out. The SSPL study allowed the identification of red, orange, green and blue emitters derived from **Eu-msucc**, **Sm-msucc**, **Tb-msucc**, **Gd-msucc**, respectively, whereas, **Nd-msucc** exhibited emissions in the near infrared region. In particular, Eu and Tb-based MOF exhibit the most promising performances in comparison with analogous phases. Due to the hypersensitive nature of the $^5D_0 \rightarrow {}^7F_2$ Eu^{3+} emission transition, **Eu-msucc** phase is proposed as a sensor model towards small molecules. An in-depth study of the energy transfer process (expressed in PL parameters such as k_{rad}, k_{nrad}, Q_{Eu}, η_{ET} and τ_{obs}) between the organic groups of protic and aprotic solvents and the emitting Eu^{3+} centers was performed. The presence of OH groups produces an efficient quenching effect which makes **Eu-msucc** a promising candidate for the development of humidity sensors.

EXPERIMENTAL SECTION

Synthesis: $[Ln_2(C_5H_6O_4)_3(H_2O)_2]$ compounds with Ln^{3+}=Nd, Sm, Eu, Gd and Tb – **Ln-msucc** –

were prepared via hydrothermal method by dissolving 1.5 mmol of methylsuccinic acid and 1 mmol of each lanthanide chloride or nitrate in 15 mL of distilled water. The pH value was adjusted to 3-4.5 with triethylamine. The mixture was stirred for 30 minutes and then heated at 180 °C in a 120 mL Teflon-lined Parr bomb. After 72 h, the reaction was immediately quenched by immersing the reactors in cold water. Finally, the products were washed with water and ethanol and dried at room temperature. For more procedure details see Sup. Inf. S15. The stoichiometries of **Ln-msucc** were confirmed by thermal and elemental analysis. Anal. Calcd. (%) for **Nd-msucc**, $Nd_2C_{15}H_{22}O_{14}$ (714.48): C :25.2, H: 3.08, O: 31.35, Found: C: 25.31, H: 3.02, O: 31.50; **Sm-msucc**, $Sm_2C_{15}H_{22}O_{14}$ (726.7): C :24.76, H: 3.03, O: 30.82, Found: C: 24.81, H: 2.99, O: 30.92; **Eu-msucc**, $Eu_2C_{15}H_{22}O_{14}$ (729.92): C :24.66, H: 3.01, O: 30.68, Found: C: 24.81, H: 2.95, O: 30.79; **Gd-msucc**, $Gd_2C_{15}H_{22}O_{14}$ (740.50): C :24.31, H: 2.97, O: 30.24, Found: C: 24.52, H: 2.89, O: 30.12; **Tb-msucc**, $Tb_2C_{15}H_{22}O_{14}$ (743.84): C :24.20, H: 2.95, O: 30.11, Found: C: 24.5, H: 2.82, O: 30.21. Additionally, semiquantitative EDS analysis were carried out (see Sup. Inf. S16).

Powder X-ray diffraction (PXRD): The X-ray diffraction pattern of **Nd-msucc** was recorded using a Bruker D8-Advance Diffractometer with Cu-Kα radiation (λ_1= 1.54056 Å, λ_2= 1.54439 Å) operating at 40 kV and 40 mA and equipped with a LynxEye detector. Horizontal slits of 0.2 mm were used in the incident beam to accurately measure the low angle reflections. The powder pattern was refined using the Rietveld method[53] as implemented in the FullProf program. [54, 55] Thompson-Cox-Hastings pseudo Voigt functions were used for describing the peak profiles.[56] For the other lanthanide-based compounds, patterns were obtained with a Rigaku D-MAX-IIIC diffractometer using CuKα radiation (λ_1= 1.54056 Å, λ_2= 1.54439 Å). ATOMS[57] and MERCURY 2.0[58] programs were used for molecular graphics for publication.

Density Functional Theory (DFT) calculations: DFT calculations were performed using the Vienna Ab-initio Simulation Package (VASP) [59]. A plane-wave basis set with an energy cutoff of 520 eV was employed, along with the Perdew-Burke-Ernzerhof (PBE) exchange-correlation functional [60]. The long-range weak dispersion interactions were taken into account using the non-local van der Waals functional optB88-vdW[61]. The electron-ion interactions were described by the projector augmented wave (PAW) method[62] in the implementation of Kresse and Joubert [63]. Lattice parameters and atomic positions were optimized until the forces on all atoms were smaller than 0.01 eV $Å^{-1}$ and SCF convergence criteria below 10^{-5} eV.

Fourier transform infrared spectroscopy (FTIR) and Raman spectroscopy: FTIR spectra were recorded with a Nicolet Protégé 460 spectrometer in the 4000-400 cm^{-1} range with 64 scans and a spectral resolution of 4 cm^{-1} by the KBr pellet technique. Raman spectrum was recorded at room temperature with a Raman Tec5 equipped with a multimode diode laser operating at 785 nm into the 3100-300 cm^{-1} range.

Thermal Analysis: Thermogravimetric Analysis (TGA) and Differential Thermal Analysis (DTA) were performed with Shimadzu TGA-51 and DTA-50 apparatus under flowing air at 50 mL min^{-1}, at a heating rate of 10 °C min^{-1}. X-ray powder diffraction was applied for further characterization of the pyrolysis products.

Scanning electron microscopy (SEM): SEM micrographs and Energy Dispersive Analysis of X-ray Spectroscopy (EDS) were obtained on FEI Quanta 200 equipment. Samples were placed on an adhesive carbon tape coated with gold.

Magnetic properties: Magnetic properties were measured on powder samples with a Quantum Design Versalab™ vibrating sample magnetometer. Measurements were performed between 50 and 300 K under the application of a magnetic field of 1 Tesla. The temperature dependence of the susceptibility was corrected using the corresponding Pascal's constants for the ligand.[64]

Solid State Luminescence Measurements: The steady state and time resolved luminescence measurements were performed on an Edinburgh Instruments FLSP920 spectrometer setup, using a 450 W xenon lamp as the steady state excitation source and a 60 W pulsed xenon lamp as the time resolved excitation source (operating at a pulse frequency of 100 Hz). The emission was detected by a Hamamatsu R928P PMT photomultiplier tube for the visible range and a Hamamatsu

R5509-72 photomultiplier operating at 193 K for the NIR range. Excitation spectra were corrected for the xenon lamp emission profile, whereas emission spectra were corrected for the detector response curve. All measurements were carried out at a step size of 0.1 nm. Time-resolved measurements were performed using a Continuum® Surelite I laser (450 mJ @1064 nm), operating at a repetition rate of 10 Hz and using the third harmonic (355 nm) as the excitation source, and the NIR photomultiplier detector mentioned above. Commission Internationale de l'Eclairage (CIE) (x,y) color coordinates were calculated using MATLAB® program.

Chemical sensor studies: The sensing activity of **Eu-msucc** was investigated monitoring the emission spectra at 611 nm, when exciting the samples at 392 nm. A quartz cuvette of 1 cm of optical path was employed. The **Eu-msucc**/solvent suspensions were prepared introducing 1 mg of powdered sample into 4 mL (0.25 $mg.mL^{-1}$) of each solvent [methanol (Carl Roth, ≥99%), ethanol (Fischer Chemical, 99.9%), dimethylformamide (Sigma Aldrich, 99.8%), acetone (Across Organics, pure), chloroform (Sigma Aldrich, ≥99.8%), n-butanol (Across Organics, 99.9%) and isopropanol (Fiers, ≥99.7%)]. The samples were previously ultrasonicated for 20 minutes. The vibrational characterization of the **Eu-succ**/solvent systems are shown in Supp. Inf. S18.

Acknowledgements

This work was supported by the Consejo Nacional de Investigaciones Científicas y Técnicas, ANPCyT PICT 2012-2087 (CNEA) and PROICO 2-1612 (UNSL-INTEQUI). G.E.G. acknowledges the postdoctoral CONICET fellowship and HYMADE project. R.V.D. thanks the Hercules Foundation (project AUGE/09/024 "Advanced Luminescence Setup") for funding. A.M.K. acknowledges Ghent University's Special Research Fund (BOF) for a Postdoctoral Mandate (project BOF15/PDO/091). C.M.-D. and G.R. acknowledge financial support from the Fondation de l'Orangerie. G.E.N. and G.J.A.A.S.I. are members of CIC-CONICET. Besides, this project has received funding from the European Union's Horizon 2020 research and innovation program H2020-MSCA-RISE-2014, GA Nº 645686.

.

Keywords: Lanthanides • Metal-Organic Frameworks • Photoluminescence • Sensors • 2-methylsuccinate

FULL PAPER

A new set of 3D luminescent lanthanide MOFs based on Nd^{3+}, Sm^{3+}, Eu^{3+}, Gd^{3+} and Tb^{3+} and flexible 2-methylsuccinate (**Ln-msucc**) was obtained and fully characterized. Magnetic properties and solid-state photoluminescence were also explored. Besides, the chemical-sensor activity of **Eu-msucc** was studied in presence of protic and aprotic solvents in terms of quenching effects and variations in values of intrinsic quantum yields, radiative and non-radiative constants, lifetimes and intensity transitions.

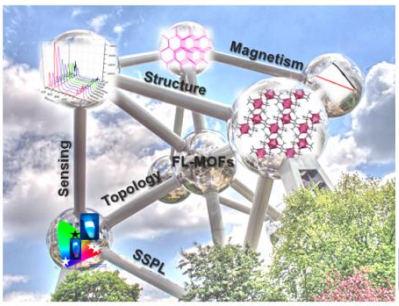

MOFs luminescence and sensing

Germán E. Gomez, Elena V. Brusau Anna M. Kaczmarek, Caroline Mellot-Drazniek, Joaquín Sacanell, Gwenaelle Rousse, Rik Van Deun, Clément Sanchez, Griselda E. Narda*, Galo J. A. A. Soler Illia**

Flexible Ligand Based Lanthanide Three-Dimensional Metal-Organic Frameworks with Tunable Solid-State Photoluminescence and OH-Solvent-Sensing Properties

References

[1] (a) J.-L. Wang, C. Wang, W. Lin, *ACS Catal.*, **2012**, *2*, 2630-2640; (b) A. Corma, H. García, F. X. Llabrés i Xamena, *Chem. Rev.*, **2010**, *110*, 4606-4655.

[2] J.-R. Li, J. Sculley, H.-C. Zhou, *Chem. Rev.*, **2012**, *112*, 869-932.

[3] (a) J.-C. G. Bünzli, S. Comby, A.-S. Chauvin, C. D. B. Vandevyver, *J. Rare Earths*, **2007**, *25*, 257-274; (b) F. Le Natur, G. Calvez, C. Daiguebonne, O. Guillou, K. Bernot, J. Ledoux, L. Le Pollès, C. Roiland, *Inorg. Chem.*, **2013**, *52*, 6720-6730; (c) X. Fan, S. Freslon, C. Daiguebonne, G. Calvez, L. Le Pollés, K. Bernot, O. Guillou, *J. Mater. Chem. C*, **2014**, *2*, 5510-5525; (d) P. G. Derakhshandeh, J. Soleimannejad, J. Janczak, A. M. Kaczmarek, K. Ven Hecke, R. Van Deun, *CrystEngComm*, **2016**, *18*, 6738-6747; (e) K. Kuriki, Y. Koike, Y. Okamoto, *Chem. Rev.*, **2002**, *102*, 2347-2356.

[4] M. H. V. Werts, *Sci. Pro.*, **2005**, *88(2)*, 101-131.

[5] J. Marling, *IEEE J. Sel. Top. Quantum Electron.*, **1978**, *14*, 56-62.

[6] A. Polman, F. C. J. M. van Veggel, *J. Opt. Soc. Am. B*, **2004**, *21*, 871-892.

[7] (a) B. W. D'Andrade, S. R. Forrest, *Adv. Mater.*, **2004**, *16*, 1585-1595; (b) H. C. Su, H. F. Chen, F. C. Fang, C. C. Liu, C. C. Wu, K. T. Wong, Y. H. Liu, S. M. Peng, *J. Am. Chem. Soc.*, **2008**, *130*, 3413-3419; (c) Y. H. Niu, M. S. Liu, J. W. Ka, J. Bardeker, M. T. Zin, R. Schofield, Y. Chi, A. K. Y. Jen, *Adv. Mater.*, **2007**, *19*, 300-304.

[8] (a) J.-C. G. Bünzli, C. Piguet, *Chem. Soc. Rev.*, **2005**, *34*, 1048-1077; (b) C. D. S. Brites, P. P. Lima, N. J. O. Silva, A. Millán, V. S. Amaral, F. Palacio, L. D. Carlos, *New J. Chem.*, **2011**, *35*, 1177-1183.

[9] Z. Hu, B. J. Deibert, J. Li, *Chem. Soc. Rev.*, **2014**, *43*, 5815-5840.

[10] D. Ananias, C. D. S. Brites, L. D. Carlos, J. Rocha, *Eur. J. Inorg. Chem.*, **2016**, 1967-1971.

[11] Z.-J. Lin, J. Lü, M. Hong, R. Cao, *Chem. Soc. Rev.*, **2014**, *43*, 5867-5895.

[12] M. C. Bernini, N. Snejko, E. Gutierrez-Puebla, E. V. Brusau, G. E. Narda, M. A. Monge, *Inorg. Chem.*, **2011**, *50*, 5958-5968.

[13] D. T. De Lill, A. Bettencourt-Dias, C. L. Cahill, *Inorg. Chem.*, **2007**, *46*, 3960-3965.

[14] (a) F. Serpaggi, G. Férey, *Microporous Mesoporous Mater.*, **1999**, *32*, 311-318; (b) A. Seguatni, M. Fakhfakh, M. J. Vauley, N. J. Jouini, *Solid State Chem.*, **2004**, *177*, 3402-3410; (c) J. Perles, M. Iglesias, C. Ruiz-Valero, N. Snejko, *J. Mater. Chem.*, **2004**, *14*, 2683-2689; (d) G.-H. Cui, J.-R. Li, R.-H. Zhang, X.-H. Bu, *J. Mol. Struct.*, **2005**, *740*, 187-191; (e) Y. F. Zhou, F. L. Jiang, D. Q. Yuan, B. L. Wu, M. C. Hong, *J. Mol. Struct.*, **2005**, *743*, 21-27; (f) M. C. Bernini, E. V. Brusau, G. E. Narda, G. E. Echeverria, C. G. Pozzi, G. Punte, C. W. Lehmann, *Eur. J. Inorg. Chem.*, **2007**, 684-693; (g) X. J. Zhang, Y. H. Xing and J. Han, *J. Coord. Chem.*, 2008, **61**, 651-653; (h) M. C. Bernini, F. Gándara, M. Iglesias, N. Snejko, E. Gutiérrez-Puebla, E. V. Brusau, G. E. Narda, M. A. Monge, *Chem. Eur. J.*, **2009**, *15*, 4896-4905; (i) C. A. F. de Oliveira , F. F. da Silva, I. Malvestiti, V. Rodrigues dos S. Malta, J. D. L. Dutra, N. B. da Costa Jr., R. O. Freire, S. Alves Jr., *J. Molecular Struc.*, **2013**, *1041*, 61-67; (j) R. F. D'vries, I. Camps, J. Ellena, *Cryst. Growth Des.*, **2015**, *15*, 3015-3023.

[15] (a) D.-X. Hu, F. Luo, Y.-X. Che, J.-M. Zheng, *Cryst. Growth Des.*, **2007**, *7*, 1733-1737; (b) M. G. Lahoud, L. F. Marques, P. B. da Silva, C. A. S. de Jesus, C. C. P. da Silva, J. Ellena, R. S. Freitas, M. R. Davolos, R. C. G. Frem, *Polyhedron*, **2013**, *54*, 1-7; (c) Y.-T. Liu, Y.-Q. Du, X. Wu, Z.-P. Zheng, X.-M. Lin, L.-C. Zhu, Y.-P. Cai, *CrystEngComm*, **2014**, *16*, 6797-6802.

[16] M. C. Bernini, V. A. de la Peña-O'Shea, M. Iglesias, N. Snejko, E. Gutierrez-Puebla, E. V. Brusau, G. E. Narda, F.Illas, M. A. Monge. *Inorg. Chem.*, **2010**, *49*, 5063-5071.

[17] P. J. Saines, M. Steinmann, J.-C. Tan, H. H.-M. Yeung, A. K. Cheetham, *CrystEngComm*, **2013**, *15*, 100-110.

[18] G. E. Gomez, M. C. Bernini, E. V. Brusau, G. E. Narda, W. A. Massad, A. Labrador, *Cryst. Growth Des.*, **2013**, *13*, 5249-5260.

[19] G. E. Gomez, M. C. Bernini, E. V. Brusau, G. E. Narda, D. Vega, A. M. Kaczmarek, R. Van Deun, M. Nazarro, *Dalton Trans.*, **2015**, *44*, 3417-3429.

[20] G. E. Gomez, A. M. Kaczmarek, R. Van Deun, E. V. Brusau, G. E. Narda, D. Vega, M. Iglesias, E. Gutierrez-Puebla, M. A. Monge, *Eur. J. Inorg. Chem.*, **2016**, 1577-1588.

[21] W. Li, P. T. Barton, M. S. R. N. Kiran, R. P. Burwood, U. Ramamurty, A. K. Cheetham, *Chem. Eur. J.*, **2011**, *17*, 12429-12436.

[22] Z.-Y. Li, B. Zhai, S.-Z. Li, G.-X. Cao, F.-Q. Zhang, X.-F. Zhang , C. Zhang, *Cryst. Growth Des.*, **2016**, *16 (8)*, 4574-4581.

[23] N. G. Connelly, T. Damhus, R. M. Hartshorn, A. T. Hutton, Nomenclature of Inorganic Chemistry - IUPAC Recommendations 2005; RSC Publishing: Cambridge, U.K., **2005**.

[24] A. K. Cheetham, C. N. R. Rao, R. K. Feller, *Chem. Comm*., **2006**, 4780-4795.

[25] (a) V. A. Blatov, IUCr Computing Commission Newsletter; IUCr: Chester, U.K., **2006**, *7*, 4-38; (b) V. A. Blatov, L. Carlucci, G. Ciani, D. M. Proserpio, *CrystEngComm*, **2004**, *6*, 377-395.

[26] N. L. Rosi, J. Kim, M. Eddaoudi, B. Chen, M. O'Keeffe, O. M. Yaghi, *J. Am. Chem. Soc*., **2005**, *127*, 1504-1518.

[27] V. A. Blatov, A. P. Shevchenko, D. M. Proserpio, *Cryst. Growth Des*., **2014**, *14*, 3576-3586.

[28] A. L. Spek, *Acta Crystallogr. Sect. A*, 1990, **46**, C34.

[29] M. J. Turner, J. J. McKinnon, D. Jayatilaka, M. A. Spackman, *CrystEngComm*, **2011**, *13*, 1804-1813.

[30] K. Nakamoto, *Infrared and Raman Spectra of Inorganic and Coordination Compounds*, John Wiley & Sons Inc., USA, **1997**.

[31] C. Benelli, D. Gatteschi, *Chem. Rev*., **2002**, *102*, 2369-2388.

[32] G. Punte, G. Echeverría, F. Sives, E. V. Brusau, J. C. Pedregosa, G. E. Narda, J. Ellena, *C. R. Chimie*, **2005**, *8*, 1469-1476.

[33] G. Echeverría, G. Punte, F. Sives, E. V. Brusau, J. C. Pedregosa, G. E. Narda, J. Ellena, *Physica B*, **2004**, *354*, 377-388.

[34] J. Xu, J. Cheng, W. Su, M. Hong, *Cryst. Growth Des*., **2011**, *11*, 2294-2301.

[35] Y. Cui, Y. Yue, G. Qian, B. Chen, *Chem. Rev*., **2012**, *112*, 1126-1162.

[36] Y. Cui, H. Xu, Y. Yue, Z. Guo, J. Yu, Z. Chen, J. Gao, Y. Yang, G. Qian, B. Chen. *J. Am. Chem. Soc.*, **2012**, *134*, 3979-3982.

[37] (a) F. Gándara, A. de Andrés, B. Gómez-Lor, E. Gutiérrez-Puebla, M. Iglesias, M. A. Monge, D. M. Proserpio, N. Snejko, *Cryst. Growth Des*., **2008**, *8*, 378-380; (b) R. F. D'vries, G. E. Gomez, J. H. Hodak, G. J. A. A. Soler-Illia, J. Ellena, *Dalton Trans.*, **2016**, *45*, 646-656.

[38] F. Tanaka, S. Yamashita, *Inorg. Chem*., **1984**, *23*, 2044-2046.

[39] P. P. Bartelemy and G. R. Choppin, *Inorg. Chem*., **1989**, *28*, 3354-3357.

[40] A.-S. Chauvin, F. Gumy, D. Imbert and J.-C. G. Bünzli, *Spectrosc. Lett.*, **2004**, *37*, 517-534.

[41] J. Scholten, G. A. Rosser, J. Wahsner, N. Alzakhem, C. Bischof, F. Stog, A. Beeby, M. Seitz, *J. Am. Chem. Soc*., **2012**, *134*, 13915-13917.

[42] *Hybrid Materials: Synthesis, Characterization, and Applications*, ed. G. Kickelbick, Wiley-VCH Verlag GmbH & Co. KGaA, Germany, 1st, **2007**, *9*, 337-374.

[43] M. D. Allendorf, C. A. Bhakta, R. J. T. Houk, *Chem. Soc. Rev.*, **2009**, *38*, 1330-1352.

[44] R. F. D'vries, G. E. Gomez, D. F. Lionello, M. C. Fuertes, G. J. A. A. Soler-Illia, J. Ellena, *RSC Adv.*, **2016**, *6*, 110171-11081.

[45] Y. Yu, J.-P. Ma, Y.-B. Dong, *CrystEngComm*, **2012**, *14 (21)*, 7157-7160.

[46] B. Chen, L. Wang, F. Zapata, G. Qian, E. B. Lobkovsky, *J. Am. Chem. Soc.*, **2008**, *130 (21)*, 6718-6719.

[47] H. Xu, X. Rao, J. Gao, J. Yu, Z. Wang, Z. Dou, Y. Cui, Y. Yang, B. Chen, G. Qian, *Chem. Commun.*, **2012**, *48 (59)*, 7377-7379.

[48] S. Pramanik, C. Zheng, X. Zhang, T. J. Emge, J. Li, *J. Am. Chem. Soc.*, **2011**, *133 (12)*, 4153-4155.

[49] C. Piguet, J.-C. G. Bünzli, G. Bernardinelli, G. Hopfgartner, A. F. Williams, *J. Am. Chem. Soc.*, **1993**, *115*, 8197-8206.

[50] (a) G. Stein, E. Wurzberg, *J. Chem. Phys*., **1975**, *62*, 208-213; (b) A. Heller, *J. Am. Chem. Soc*., **1966**, *88*, 2058-2059.

[51] J.-M. Zhou, W. Shi, N. Xu, P. Cheng, *Inorg. Chem*., **2013**, *52*, 8082-8090.

[52] (a) B. Chen, Y. Yang, F. Zapata, G. Lin, G. Qian, E. B. Lobkovsky, *Adv. Mater*., **2007**, *19*, 1693-1696; (b) S. Dang, X. Min, W. Yang, F.-Y. Yi, H. You, Z.-M. Sun, *Chem. Eur. J*., **2013**, *19*, 17172-17179.

[53] H. M. Rietveld, *J. Appl. Crystallogr.*, **1969**, *2*, 65-71.

[54] J. Rodríguez-Carvajal, *Physica B*, 1993, **192**, 55-56.

[55] J. Rodríguez-Carvajal, FullProf Suite, www.ill.eu/sites/fullprof/.

[56] L. W. Finger, D. E. Cox, A. P. Jephcoat, *J. Appl. Crystallogr.*, **1994**, *27*, 892-900.

[57] E. Dowty, ATOMS for Windows, a computer program for displaying atomic structure, Version 3.1, Shape Software, Kingsport, TN, **1995**.

[58] C. F. Macrae, I. J. Bruno, J. A. Chisholm, P. R. Edgington, P. McCabe, E. Pidcock, L. Rodriguez-Monge, R. Taylor, J. van de Streek, P. A. Wood, Mercury CSD 2.0 - new features for the visualization and investigation of crystal structures, *J. Appl. Crystallogr.*, **2008**, *41*, 466-470.

[59] (a) G. Kresse, J. Furthmüller, *Comput. Mater. Sci.*, **1996**, *6*, 15-50; (b) G. Kresse, J. Furthmüller, *Phys. Rev. B*, **1996**, *54*, 11169-11186.

[60] J. P. Perdew, K. Burke, M. Ernzerhof, *Phys. Rev. Lett.*, **1996**, *77*, 3865-3868.

[61] (a) J. Klimes, D. R. Bowler, A. Michaelides, *Phys. Rev. B: Condens. Matter Mater. Phys.*, **2011**, *83*, 195131-195144; (b) D. C. Langreth, B. I. Lundqvist, S. D. Chakarova-Kack, V. R. Cooper, M. Dion, P. Hyldgaard, A. Kelkkanen, J. Kleis, L. Z. Kong, S. Li, P. G. Moses, E. Murray, A. Puzder, H. Rydberg, E. Schroder, T. Thonhauser, *J. Phys.: Condens. Matter.*, **2009**, *21*, 084203.

[62] P. E. Blöchl, *Phys. Rev. B*, **1994**, *50*, 17953-17979.

[63] G. Kresse, D. Joubert, *Phys. Rev. B*, 1999, **59**, 1758-1775.

[64] G. A. Bain, J. F. Berry, *J. Chem. Educ.*, **2008**, *85*, 532-536.